



1 **Can Aerosols improve Urban Flood Prediction? A case study of**
2 **2015 Chennai extreme event**

3

4 Oscar Paul¹, N. Nithila Devi^{1,2}, Rakesh Teja Konduru³, Soumendra Nath Kuiry¹, Kundan Lal
5 Shrestha⁴ and Chandan Sarangi¹

6

7 ¹ Department of Civil Engineering, Indian Institute of Technology Madras, Chennai, Tamil Nadu, India

8 ² Section 4.4: Hydrology, GFZ Helmholtz Centre for Geosciences, Potsdam, Germany

9 ³ Earth Observation Research Center, Japan Aerospace Exploration Agency (JAXA), Tsukuba Space Center, Tsukuba,
10 Ibaraki, Japan

11 ⁴ Department of Chemical Science and Engineering, Kathmandu University, Dhulikhel, Nepal

12
13 *Correspondence to:* Chandan Sarangi (chandansarangi@civil.iitm.ac.in)

14

15

16 **Abstract.** In December 2015, Chennai, a coastal megacity in India, faced an extreme precipitation-flooding event
17 (EPF) that triggered a devastating 1-in-100-year flood. Several previous attempts failed to accurately simulate the
18 spatiotemporal variability of this EPF at the urban basin scale. Even though incorporating aerosols into operational
19 weather models can improve the accuracy of EPF simulations, it is often ignored due to its computational cost. To
20 address this, we conducted ensemble experiments to highlight the significance of aerosol-cloud interactions in
21 simulating this EPF. In that regard, we use a computationally intensive, high-resolution WRF model configured in
22 large-eddy simulation (LES) mode to represent the interactions in the complex urban microphysics. The results
23 indicate that explicit aerosol representation significantly influenced the microphysics-dynamics interaction during the
24 2015 EPF and produced rainfall patterns in closer agreement with satellite and rain gauge observations, with basin-
25 scale improvement of ~22%. Further, employing simulated rainfall in a coupled hydrologic-hydraulic modeling
26 framework increased inundation accuracy by ~50%. Thus, this study suggests that explicit aerosol representation can
27 improve the space-time simulation of rainfall and flooding for the EPF in Chennai and potentially for similar coastal
28 megacities.

29

30

31

32

33

34

35

36

37

38



1

2 **1 Introduction**

3 Observations from recent decades reveal a distinct increase in the frequency and magnitude of extreme precipitation
4 events over India (Goswami et al., 2006; Mishra and Shah, 2018; Pattanaik and Rajeevan, 2010; Roxy et al., 2017).
5 This has increased concerns about severe urban flooding, which often results in significant loss of life and property.
6 Hence, accurate numerical simulation and forecasting of extreme precipitation-flooding (EPF) events are essential for
7 urban flood management using the EPF forecasting frameworks, which couple atmospheric, hydrological, and
8 hydraulic models (Ghosh et al., 2019). Nevertheless, considering the complex nonlinear interactions between regional
9 meteorology, cloud microphysics and dynamics, and urban-scale land-atmosphere interactions at different spatio-
10 temporal scales within the atmospheric models makes it challenging. High-resolution cloud-resolving atmospheric
11 models are demonstrating improved accuracy in simulations of heavy precipitation at regional scale (Hazra et al.,
12 2017; Konduru et al., 2023; Barros et al., 2018; Sarangi et al., 2017; Sarangi, et al., 2018). However, accurately
13 capturing the spatiotemporal variability in extreme precipitation over urban basins remains a challenge, so does EPF
14 forecasting. Specifically, the biases in simulated spatiotemporal rainfall patterns over the urban basins propagate into
15 the flood forecasting system and impact the accuracy of runoff streamflow, and flood inundation predictions over
16 megacities (Gomez et al., 2019). This significantly impacts the community's flood preparedness, as the flood hazard
17 and damage assessment depend on the simulated flood depth and inundation extent.

18 Often, extreme precipitation events occur during monsoon season in India. Based on long-term observational and
19 simulation experiments, recent studies have revealed the strong influence of aerosols on extreme rainfall
20 characteristics over India through aerosol-cloud-rain processes (Rai et al., 2023). Delayed collision-coalescence in
21 warm clouds elevates condensate to mixed-phase levels, resulting in the formation of larger hydrometeors. This results
22 in delayed but intensified precipitation over the region (Sarangi et al., 2017; Sarangi, Kanawade, et al., 2018; Sarangi,
23 Tripathi, et al., 2018). However, it is uncertain whether such aerosol-cloud-rain processes play a significant role in
24 rainfall simulation at spatial scales of urban basins (i.e., 5-15 km²). This uncertainty arises partly from the sensitivity
25 of cloud microphysical processes to internal model variability (IMV), with initialization at the onset of convective
26 intensification being critical for accurately capturing extreme event intensity (Tewari et al., 2022). Hence,
27 incorporating urban aerosols into operational numerical weather prediction at the urban basin scale is largely ignored
28 , as coupled microphysics-meteorology forecasting is computationally exhaustive and time-consuming.

29 An EPF event (December 1, 2015) occurred over Chennai, a coastal megacity in India, which is considered as a 1-in-
30 100-year return period flood. The event had reported maximum daily rainfall of ~500 mm over the basin. Hence, it is
31 one of the most catastrophic urban flooding events in over a century, causing an estimated 500 fatalities and a 3 billion
32 USD loss (Nithila Devi et al., 2019). Many modeling studies have simulated this event, but these studies have high
33 biases in the simulated spatiotemporal variability of the storm and resulting rainfall over the basin. While some studies
34 highlighted the influence of synoptic-scale convective systems linked to El Niño and Rossby wave shifts (Chakraborty,
35 2016), some attributed the warming trend of sea-surface temperature in the Bay of Bengal (Boyaj et al., 2018; Panda
36 and Rath, 2022; van Oldenborgh et al., 2016). Others indicated that the local drivers like orography (Phadtare, 2018),



1 improving boundaries (Rath and Panda, 2019; Srinivas et al., 2018), cloud microphysics (Reshmi Mohan et al., 2018)
2 processes and use of realistic urban land use (Konduru et al., 2023; Panda and Rath, 2022) can improve the
3 spatiotemporal pattern of rainfall of this event. However, despite these insights, the lack of aerosol-cloud processes in
4 the aforementioned studies can be one of the reasons for the underestimation of the magnitude of extreme precipitation
5 in the urban basin. Additionally, previous studies have highlighted how errors in short-range rainfall forecasts affected
6 the accuracy of 2015 flood inundation predictions for Chennai city in the Adyar basin (Nithila Devi and Kuiry, 2023).
7 These concerns underscore the importance of having accurate spatial and temporal rainfall simulations for better
8 accuracy in urban flood prediction.

9 Overall, despite the growing use of computationally intensive high-resolution WRF and LES simulations to improve
10 flood management, accurate spatiotemporal rainfall prediction at complex urban scales remains challenging.
11 Therefore, this study aims to test a focused hypothesis: Do aerosol concentrations improve the rainfall and urban flood
12 prediction of the Chennai 2015 EPF? To evaluate this hypothesis, we employed a one-way coupled atmospheric-
13 hydrologic-hydraulic modeling framework for the 2015 EPF event in Chennai. We conducted a series of aerosol
14 sensitivity experiments to quantify their effect on simulated rainfall under IMV and how these aerosol-induced
15 changes propagate into flood prediction, as detailed in Sect. 2.

16 **2 Models and experiments**

17 **2.1 Atmospheric simulations using WRF model and sensitivity experiments**

18 Weather Research and Forecasting (WRF) (Skamarock et al., 2008) is configured to perform a high-resolution
19 simulation with five interactive nested domains (27, 9, 3, 1, and 0.2 km) and 72 vertical levels (Figs. 1a and 1b). The
20 initial and boundary conditions for these simulations are obtained from the Indian Monsoon Data Assimilation and
21 Analysis (IMDAA) data (Rani et al., 2021), available at a 12 km resolution every 6 hours. The Grell-Freitas ‘scale-
22 aware’ cumulus scheme (Grell and Freitas, 2014) is applied in the 27 km and 9 km domains, while the inner three
23 domains explicitly resolve convection at 3 km, 1 km, and 0.2 km. The Mellor-Yamada Nakanishi and Niino (MYNN)
24 level 2.5 closure scheme (Nakanishi and Niino, 2009) is implemented for the planetary boundary layer (PBL)
25 processes in the outer four domains. However, the innermost domain of 0.2 km is configured in the large-eddy
26 simulation (LES) mode, without any PBL parameterization scheme. Additional model physics includes the RRTMG
27 scheme for both longwave and shortwave radiative transfer (Mlawer et al., 1997) and MM5 similarity theory for
28 estimating surface heat and moisture fluxes.

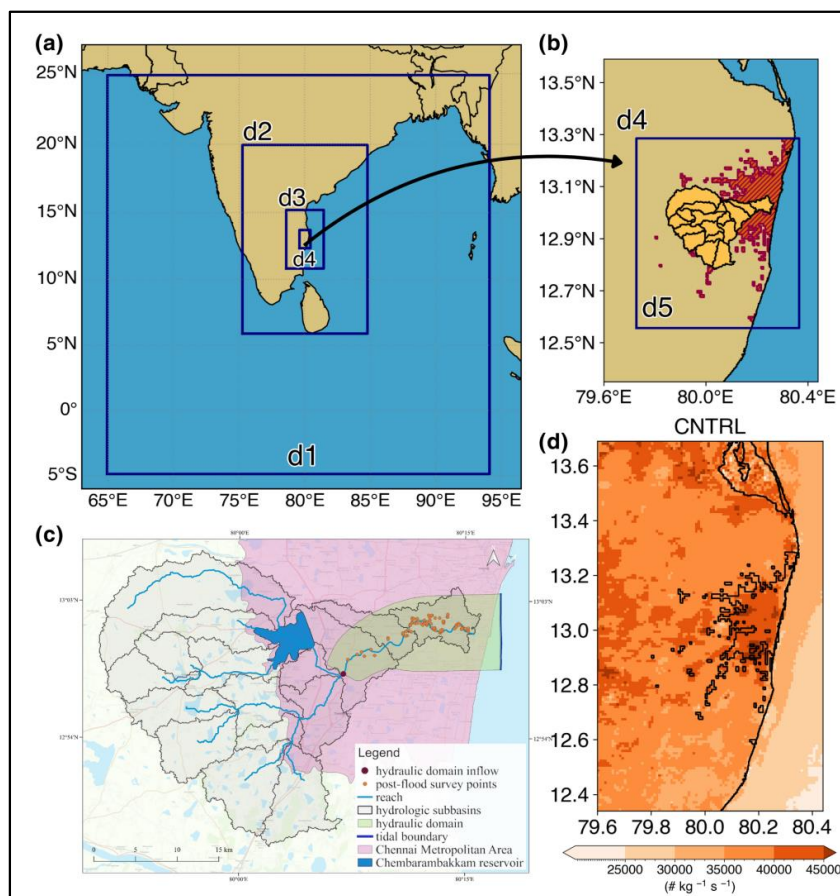
29 An updated two-moment Thompson aerosol-aware microphysics scheme (Thompson and Eidhammer, 2014) is
30 employed to incorporate the influence of aerosols via cloud condensation nuclei (CCN) and ice-nucleating (proxy for
31 IN) aerosols into the model. Land surface processes across all domains are represented using Noah-LSM (Chen and
32 Dudhia, 2001) coupled with a single-layer urban canopy model (Kusaka et al., 2001; Kusaka and Kimura, 2004). The
33 CCN concentrations are estimated from the aerosol mixing ratios obtained from Modern-Era Retrospective analysis
34 for Research and Applications (MERRA-2) (Buchard et al., 2017) reanalysis data at a relatively fine resolution of 0.5°



1 $\times 0.625^\circ$. The MERRA-2 reanalysis data of mixing ratios for sea salts and dust, along with other hydrophilic and
2 hydrophobic aerosol components, were converted into number concentrations (Lu et al., 2022) and subsequently into
3 CCN emission (Thompson and Eidhammer, 2014). In our analysis, we considered 15 years (2003-2017) of
4 climatological mean CCN concentrations, which provided CCN emissions to the WRF model. To generate spatial
5 heterogeneity in CCN emissions over Chennai, we integrated MERRA2-derived CCN with a spatial pattern obtained
6 from mean 1-km Aerosol Optical Depth data from the Multi-Angle Implementation of Atmospheric Correction
7 (MAIAC) algorithm (Lyapustin et al., 2018). This data, averaged for November-December months of 2014-2016,
8 undergoes Radial Basis Function interpolation (Zou et al., 2013) using the SciPy package (Virtanen et al., 2020). This
9 approach ensures realistic spatial heterogeneity in the magnitude of CCN emissions.

10 We performed three aerosol sensitivity experiments, with sequentially reducing CCN emission and concentrations
11 (Table S1). The baseline case (CNTRL) was followed by low-CCN case (LCCN10) with reduction factor of 10 and a
12 very-low-CCN (LCCN100) case at one-hundredth with all other model configurations held constant. The motivation
13 for these aerosol sensitivity experiments is that the climatological CCN values used in the CNTRL scenario (Fig. 1d)
14 might not ideally represent conditions prior to the EPF event in Chennai. In multiple studies, the period from
15 November 29 to December 3, 2015, is identified as the precipitation period for the 2015 event (Konduru et al., 2023;
16 Narasimhan et al., 2016). Thus, by 29 November, the influence of the ‘below-cloud scavenging’ (BCS) mechanism
17 must have resulted in relatively cleaner conditions (compared to the climatology mean). Based on the Laakso et al.
18 (2003) scavenging parameterization, continuous rainfall of 2-4 mm hr⁻¹ over 24 hours is estimated to reduce
19 accumulation-mode aerosol concentrations by factors of ~26-180, corresponding to 96-99% removal via wet
20 scavenging. Furthermore, several raingauge stations recorded extreme rainfall exceeding 30-40 mm hr⁻¹ on December
21 1, 2015, indicating even higher scavenging efficiency. Thus, the LCCN sensitivity experiments were designed to
22 simulate cleaner, more representative pre-event atmospheric conditions.

23 To assess the robustness of the aerosol-sensitivity results and to account for IMV within WRF, an ensemble approach
24 was employed at 1-km resolution (d4). Rainfall was simulated for the period 30 November 00 UTC to 2 December 00
25 UTC, with three ensemble members generated for each aerosol scenario using different lead times of 27, 24, and 21
26 hours, resulting in nine simulations in total. This ensemble framework (CNTRL-Ens, LCCN10-Ens, LCCN100-Ens)
27 enables a more reliable evaluation of how aerosol loading affects rainfall over the urban basin during the EPF event.



1

2 **Figure 1** WRF simulation domains, emission distribution, and HEC-HMS, HEC-RAS domain for Flood Analysis. (a)
 3 The nested parent domains used in WRF simulations. (b) The inner domains (d4 and d5) with urban land use and
 4 Adyar basin. (c) The delineated basin and stream network in HEC-HMS, as well as the hydraulic domain and boundary
 5 conditions for HEC-RAS. It also shows the locations where the post-flood survey was conducted to obtain the
 6 maximum inundation depths for the 2015 floods. (d) CCN surface emissions with urban land use for CNTRL in d4.

7

8 **2.2 One-way Coupled Atmospheric-Hydrologic-Hydraulic Modeling Framework**

9 Chennai city is located in the Adyar basin (Fig. 1c), through which the Adyar River flows and discharges into the Bay
 10 of Bengal. The hydrological model, HEC-HMS, is set up for the Adyar basin to simulate inflow for different scenarios
 11 into the Chembarambakkam reservoir that is located upstream of the city, and also the upstream boundary condition
 12 (marked as ‘hydraulic domain inflow’ in Fig. 1c) for the hydraulic model, HEC-RAS. The Curve Number (CN) and
 13 kinematic wave routing methods are used to estimate the effective runoff from precipitation and to route the riverine
 14 flow in the basin. The CN method utilizes soil and land use/land cover data from the National Bureau of Soil Sciences,



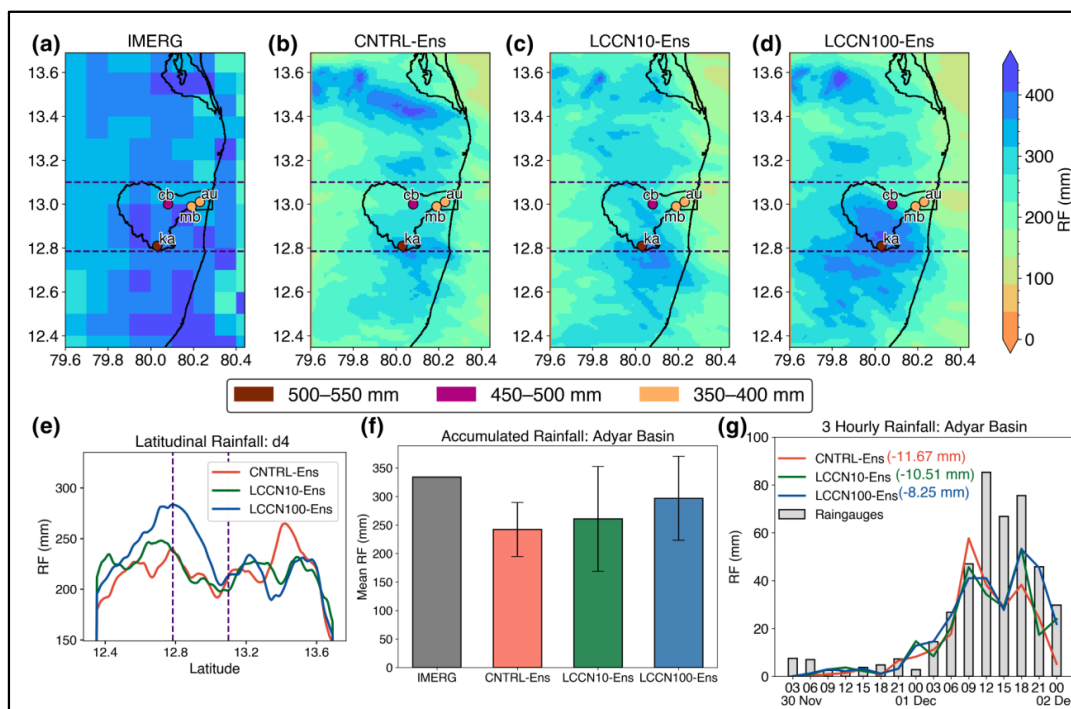
1 Pune, India, and Landsat 8, respectively. The two-dimensional HEC-RAS model routes the inflow hydrographs from
2 the HEC-HMS model through the Adyar River and obtains the flood inundation extents in the city limits. To represent
3 the complex urban terrain of Chennai, the 2 m × 2 m high-resolution LIDAR DEM data for Chennai city is used for
4 hydraulic modeling. For a better representation of flooding in the urban area of Chennai, the building footprints are
5 obtained from the Open Street Map (<https://www.openstreetmap.org>) and according to the Building Block (Brown et
6 al., 2007; Hunter et al., 2008; Schubert and Sanders, 2012) method, the values of DEM pixels corresponding to the
7 footprints are increased by 5 m to maintain no-flow condition through the buildings. More details of the hydrological-
8 hydraulic model set-up and its calibration for the 2015 EPF can be found in earlier studies (Nithila Devi et al., 2019).
9 For the hydrological and hydraulic analyses, which are highly sensitive to rainfall magnitude, a single ensemble
10 member was selected based on its spatio-temporal performance. LES simulations (d5) for rainfall were then conducted
11 for all aerosol scenarios (CNTRL-LES, LCCN10-LES, LCCN100-LES) and were one-way coupled to the hydrologic-
12 hydraulic setup (i.e., HEC-HMS and HEC-RAS). The detailed description of all simulations is provided in Table S1.

13 **3 Results**

14 **3.1 Evaluation of Ensemble mean Rainfall Simulations**

15 Figures 2a-d present the spatiotemporal distribution of ensemble-mean accumulated precipitation for the sensitivity
16 experiments, and its corresponding evaluation against IMERG satellite observations. IMERG revealed that this heavy
17 rainfall was mostly centered over the southern half of the Adyar basin, extending to regions further south (Fig. 2a).
18 The Adyar basin experienced significant rainfall on December 1, with in situ rain gauge data recorded precipitation
19 of 494 mm at Kattupakkam (ka) and 427 mm at Chembarambakkam (cb), respectively (Fig. 2).

20 In the CNTRL-Ens case, the maximum accumulated precipitation over the basin is approximately 270 mm, with a
21 significant fraction falling outside the basin boundary in the north near 13.5° N (Fig. 2b). In comparison, LCCN10-
22 Ens simulation demonstrates improvement in spatial distribution, with an increased Adyar basin-maximum of ~295
23 mm (Fig. 2c). LCCN100-Ens exhibits further enhancement of the ensemble-mean rainfall, producing a maximum
24 precipitation of ~370 mm within the basin (Fig. 2d). The latitudinal rainfall distribution (Fig. 2e) captures this gradual
25 improvement, with the peak rainfall region strengthening over the south of Adyar basin as we move from CNTRL-
26 Ens to LCCN10-Ens to LCCN100-Ens, and the northern peak weakens correspondingly. Figure 2f presents the basin-
27 averaged accumulated precipitation from IMERG along with the ensemble-mean values and associated ensemble
28 spread for all the sensitivity experiments. IMERG indicates a basin-mean accumulation of 334 mm. The ensemble-
29 mean basin-averaged precipitation is 242 mm for CNTRL-Ens, 260 mm for LCCN10-Ens, and 297 mm for LCCN100-
30 Ens. The maximum basin-averaged totals within the ensemble members are 289 mm, 352 mm, and 370 mm for
31 CNTRL-Ens, LCCN10-Ens, and LCCN100-Ens, respectively, demonstrating a systematic enhancement in the
32 representation of rainfall over the Adyar basin across the three scenarios.



1

2 **Figure 2** Spatio-temporal distribution of rainfall across sensitivity experiments (dotted lines indicate basin extent).
 3 Panels show: (a) IMERG-derived accumulated rainfall, (b-d) Accumulated rainfall from CNTRL-Ens, LCCN10-Ens,
 4 and LCCN100-Ens, respectively, with rain gauge locations and observed totals at Kattupakkam (ka),
 5 Chembarambakkam (cb), Meenambakkam (mb), and Anna University (au) within the basin. (e) Latitudinal
 6 distribution of accumulated rainfall. (f) Basin-averaged accumulated rainfall from IMERG and sensitivity
 7 experiments (error bars showcasing variation in ensemble members) (g) 3-hourly temporal rainfall patterns with mean
 8 biases at Adyar basin. An average of four rain gauges have been used for temporal comparison.

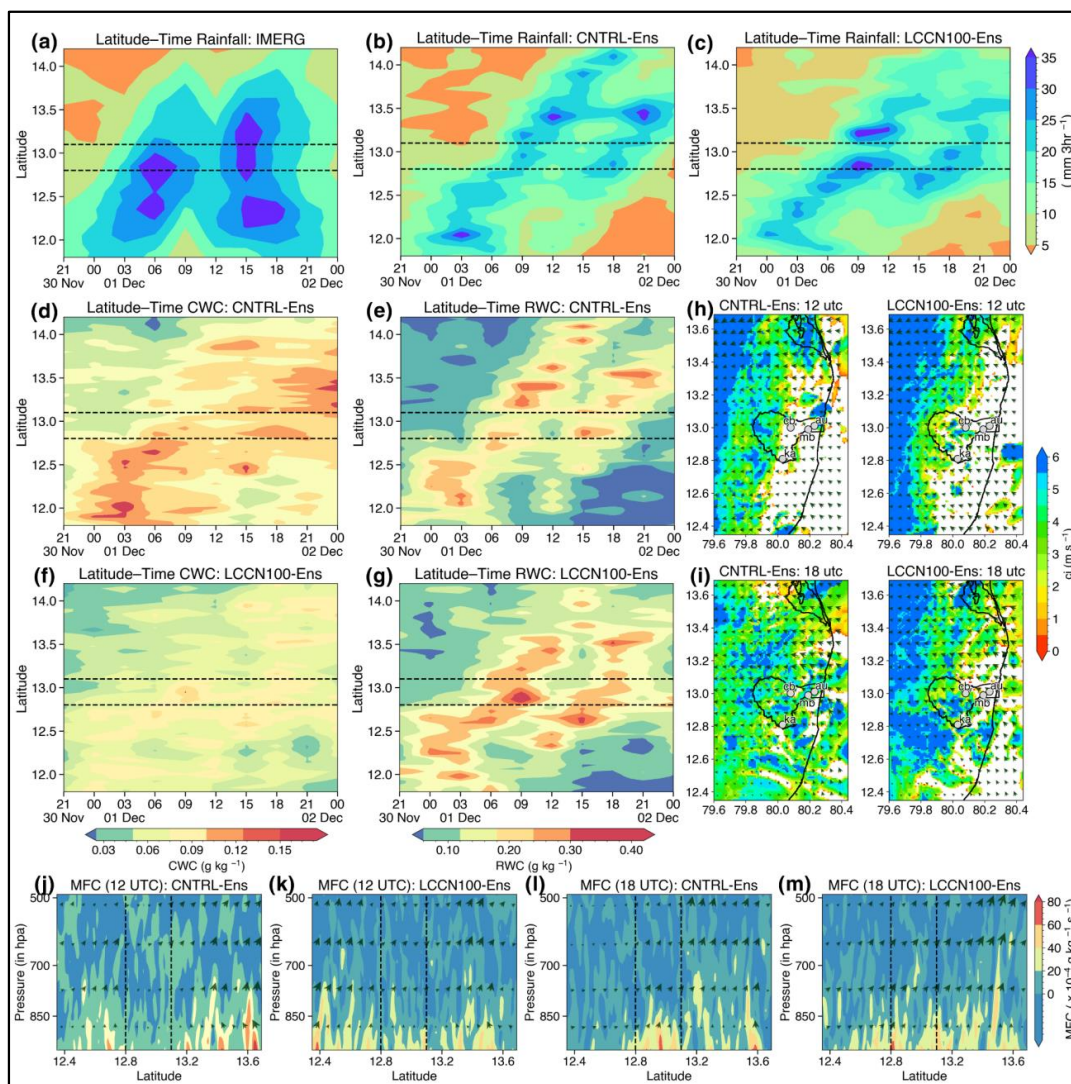
9 At the same time, the temporal variability of precipitation within the Adyar basin is also validated using in situ rain
 10 gauges (Fig. 2g). Rainfall records averaged across four gauge stations (ka, cb, mb, and au; locations shown in Fig. 2)
 11 indicate that the most intense rainfall phase in the basin occurred between 09 UTC and 21 UTC. The ensemble-mean
 12 temporal profiles from all sensitivity experiments show a distinct bimodal distribution during this period, consistent
 13 with the IMERG observations within the basin (Fig. 3a). LCCN100-Ens exhibits the lowest temporal bias (-8.25 mm),
 14 followed by LCCN10-Ens (-10.51 mm) and CNTRL-Ens (-11.67 mm) (Fig. 2f). Although all simulations show a
 15 bimodal structure, the enhanced performance of LCCN10-Ens and LCCN100-Ens arises from their improved
 16 representation of the temporal peaks, particularly the second peak during the period of intense rainfall. The first peak
 17 at 09 UTC is comparable across simulations, with 3-hourly rainfall values of ~57 mm (CNTRL-Ens), ~46 mm
 18 (LCCN10-Ens), and ~42 mm (LCCN100-Ens). However, a clear distinction appears at the second peak around 18
 19 UTC, where LCCN10-Ens and LCCN100-Ens (~53 mm) outperform CNTRL-Ens (~38 mm). This advantage persists
 20 and increases during later hours, resulting in accumulated ensemble-mean rainfall differences of ~18 mm for
 21 LCCN10-Ens and ~55 mm for LCCN100-Ens relative to CNTRL-Ens. Figs. S1 and S2 show that these rainfall
 22 differences are consistent across all ensemble members. To better understand the spatiotemporal rainfall improvement



1 in LCCN100-Ens over the Adyar Basin, we analyze the aerosol-induced changes in simulated storm morphology and
2 cloud microphysical characteristics relative to CNTRL-Ens during the entire rainfall spell on December 1 (Fig. 3).

3 IMERG surface rainfall observations on a latitudinal-temporal axes highlights a northward propagation of
4 the storm during this event, with peak precipitation over the Adyar basin at 06 UTC and 15 UTC on December 1 (Fig.
5 3a). Both CNTRL-Ens (Fig. 3b) and LCCN100-Ens (Fig. 3c) successfully capture this northward shift. However,
6 LCCN100-Ens better represents the rainfall magnitudes in and around the basin with peak rainfall observed during
7 09-12 UTC and 18-21 UTC, contributing to relatively improved simulation of the observed bimodal temporal pattern
8 in IMERG. In contrast, CNTRL-Ens simulates rainfall more to the north of the basin, with maxima near 13.5° N at
9 12 UTC and 21 UTC, consistent with the accumulated pattern shown in Figs. 2b and 2e.

10 Comparison of altitude-averaged (surface-500 hPa) cloud water content (CWC) over the basin is consistently higher
11 in CNTRL-Ens than in LCCN100-Ens throughout the event (Figs. 3d and 3f). During 00-06 UTC on 1 December,
12 CNTRL-Ens simulates CWC values of ~0.12-0.15 g kg⁻¹, nearly twice that in LCCN100-Ens (~0.06-0.09 g kg⁻¹). This
13 contrast continues as the storm enters the basin during 06-09 UTC and continues through the later stages of the event
14 (18-21 UTC). The enhanced CWC in CNTRL-Ens relative to LCCN100-Ens is accompanied by comparatively lower
15 rainwater content (RWC), which remains around 0.3 g kg⁻¹ with localized higher values in the basin at 6 UTC and 15
16 UTC (Fig. 3e). In contrast, LCCN100-Ens exhibits values exceeding 0.4 g kg⁻¹ gradually propagating into the southern
17 part of the basin by 09 UTC. A similar evolution was observed in later hours, with higher RWC south of the basin at
18 15 UTC and subsequent expansion into the basin between 15-18 UTC (Fig. 3g).



1

2 **Figure 3** Aerosol-Induced Convection in the Region (dotted lines indicate basin extent). The top row indicates
 3 latitude-temporal precipitation for (a) IMERG (b) CNTRL-Ens and (c) LCCN100-Ens from 30 November 21 UTC-2
 4 December 00 UTC. The two middle rows (left and middle columns) show altitude-averaged latitude-time variations
 5 of (d,f) cloud water (CWC) and (e,g) rainwater content (RWC) for CNTRL-Ens (d-e) and LCCN100-Ens (f-g) during
 6 the same period. The right column displays the spatial distribution of cold pool intensity for CNTRL-Ens and
 7 LCCN100-Ens at (h) 12 and (i) 18 UTC. In the bottom row, panels present longitude-averaged latitude-altitude
 8 profiles of moisture flux convergence and winds at the 12 UTC (j-k) and 18 UTC (l-m) on 1 December for CNTRL-
 9 Ens (j, l) and LCCN100-Ens (k,m).

10
 11
 12



1 As expected, lower CCN concentrations in LCCN100-Ens simulates larger droplets and enhance collision-coalescence
2 (Sarangi and Tripathi, 2018). This accelerates raindrop growth and supports the early RWC enhancement observed
3 during 06-09 UTC as the storm approaches the southern basin boundary. In contrast, CNTRL-Ens exhibits a larger
4 CWC to RWC ratio under higher aerosol loading, favoring northward propagation of convection during the same
5 period. In LCCN100-Ens, the southward enhancement of RWC during 06-09 UTC intensifies cold-pool activity
6 around the basin, strengthening cold-pool-driven updrafts and moisture content (Fig. S3). These processes collectively
7 maintain peak rainfall within and near the basin through 12 UTC without any northward movement.

8 The intensified rainfall at 12 UTC further amplifies cold-pool strength and moisture-updraft interactions around the
9 basin. At 12 UTC, the spatial distribution of cold-pool intensity (Fig. 3h) shows a domain-wide band of strong cold-
10 pool signatures between 79.6-79.8°E in LCCN100-Ens, whereas CNTRL-Ens concentrates stronger cold pools farther
11 north. Consequently, LCCN100-Ens produces greater moisture-flux convergence in and around the basin at 12 UTC
12 (Fig. 3j), while CNTRL-Ens exhibits higher convergence primarily north of the basin (Fig. 3k). This setting facilitates
13 RWC and surface rainfall south of the basin at 15 UTC in LCCN100-Ens, followed by northward progression into the
14 basin by 18 UTC as cold-pool strength remains elevated (Fig. 3i). Moisture convergence correspondingly intensifies
15 around the basin at 18 UTC (Fig. 3m), in contrast to the more scattered and weaker signals in CNTRL-Ens (Fig. 3l).
16 These processes collectively explain the stronger rainfall during 18-21 UTC in LCCN100-Ens. Overall, the reduced
17 CCN concentrations in LCCN100-Ens enhances microphysics-dynamics interaction in the region, improving the
18 basin's rainfall representation.

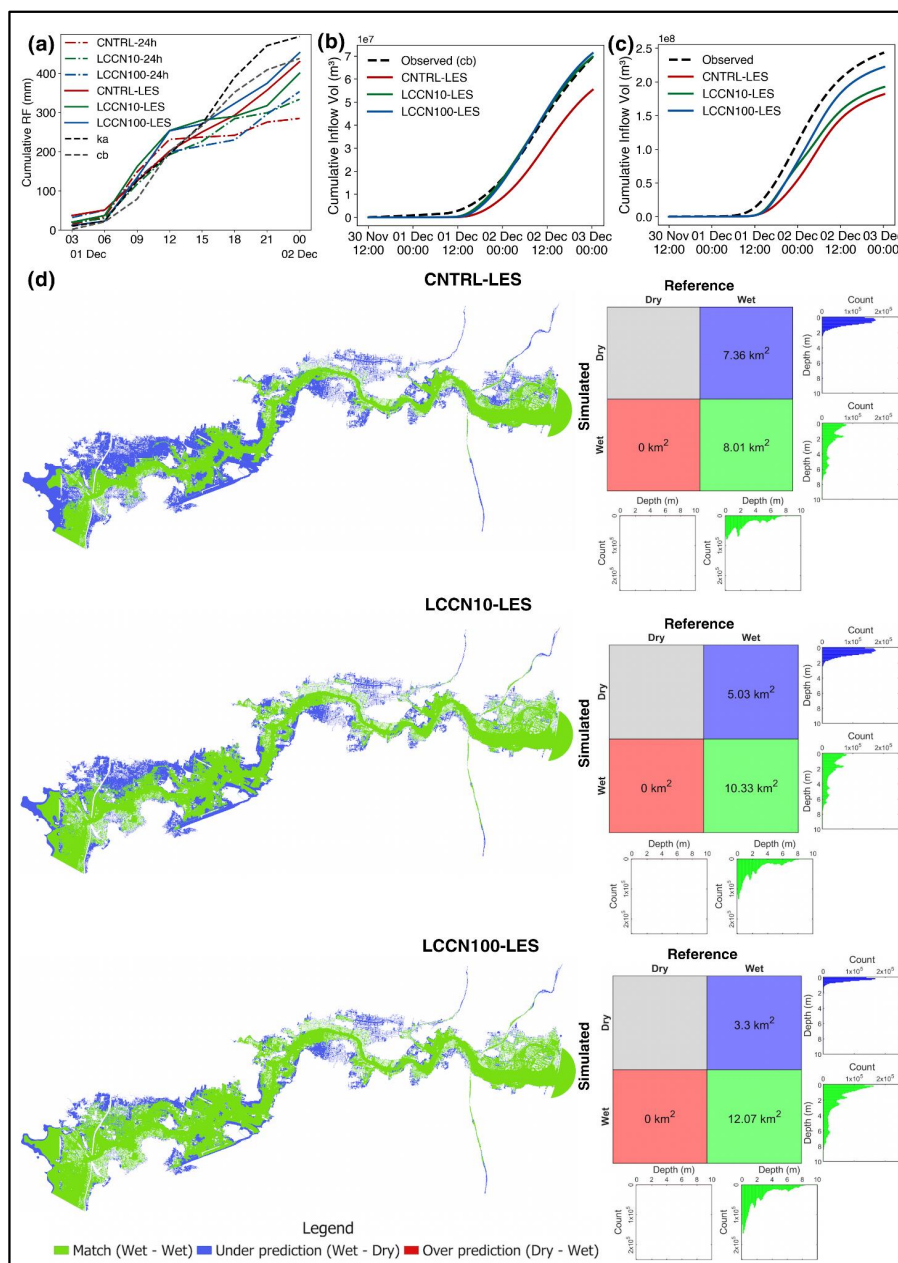
19 **3.2 Evaluation of Rainfall simulations in simulating flood discharges, depths, and extents**

20 Hydrological and hydraulic simulations are carried out to determine whether the improved spatio-temporal rainfall
21 distribution from the aerosol-sensitivity experiments are reflected into corresponding changes in reservoir inflow and
22 flood simulations. Since the Adyar basin is ungauged, hydrological simulation errors are evaluated by comparing
23 simulated inflows into the Chembarambakkam (cb) reservoir (Fig. 1c) and the Chennai city (marked as 'hydraulic
24 domain inflow' in Fig. 1c) with observed inflows during the 2015 EPF (details in Nithila and Kuiry, 2025). Among
25 the WRF ensemble simulations, the 24-hour lead-time member (CNTRL-24h, LCCN100-24h, LCCN10-24h) is
26 selected based on the best spatio-temporal performance in 1-km runs (Figs. S1-S2; Table S2). Aerosol-sensitivity LES
27 simulations are then conducted using the same model configuration. These simulations improve both the basin-wide
28 cumulative rainfall on 1 December and the temporal evolution of rainfall for LCCN10-LES and LCCN100-LES
29 relative to the corresponding 1-km simulations (LCCN10-24h and LCCN100-24h), with LCCN100-LES showing the
30 closest alignment with rain gauge observations (Fig. 4a).

31 The improved rainfall representation influences the cumulative inflow volume into the cb reservoir (Fig. 4b) and
32 Chennai city (Fig. 4c). For the cb reservoir, cumulative inflow errors decreased to 14.8% and 13.8% in the LCCN10-
33 LES and LCCN100-LES, respectively, while errors for Chennai city reduced to 20.8% and 9.4%. These improvements
34 are substantial compared with errors of 30.1% and 24.9% obtained in the CNTRL-LES. The timing of peak inflows
35 is also more accurately captured in the LCCN experiments during the EPF event (Fig. S4). Such improvements in



1 inflow prediction had an influence in the downstream flooding during the event. The inundation simulated based on
2 IMERG rainfall is closer to that from the rain gauge data (Nithila Devi et al., 2020) and is considered as the reference
3 for evaluating the inundation extents from CNTRL-LES, LCCN10-LES and LCCN100-LES rainfall inputs till 2
4 December 00 UTC. Although we were unable to secure satellite-derived inundation extents, the hydraulic simulation
5 was validated using post-flood survey depths collected closer to the Adyar River. Therefore, it can be used as a
6 reference for accuracy assessment (Nithila Devi et al., 2020). Figure 4d showcases the confusion matrix of the area
7 and depth distribution for the experiments. It categorizes the simulated results as correctly simulated (wet in both
8 observed and simulated), underpredicted (wet in observed but dry in simulated), and overpredicted (dry in observed
9 but wet in simulated) relative to the reference in the corresponding computational cells. LCCN10-LES and LCCN100-
10 LES exhibit flood extents of 10.33 km² and 12.07 km² respectively demonstrating the closest alignment with the
11 reference maximum inundation area of 15.37 km². These represent ~29% and ~51% improvements over the CNTRL-
12 LES's 8.01 km² simulated flood extent. We have quantified the accuracy of predicted flood inundation extent using
13 fitness index scores (Kuiry et al., 2010). It reported values of 0.52 for CNTRL-LES, 0.67 for LCCN10-LES, and 0.78
14 for LCCN100-LES. These results emphasize the enhanced accuracy of LCCN experiments in simulating flood
15 inundation depth and extent.



1

2 **Figure 4** Composite analysis of LES simulations, inflows and inundation depths for all the aerosol-sensitivity
 3 experiments. (a) Cumulative rainfall over the Adyar Basin from the LES runs compared with the best ensemble
 4 member. The cumulative inflow volume from IMERG and simulated inflows (b) into cb reservoir and (c) into Chennai
 5 city. (d) The inundation depth for these simulations alongside a confusion matrix depicting the pixel count and depth
 6 distribution with the reference values from IMERG data till 2 December 00 UTC.

7



1 4 Discussion and Implications

2 Ensemble experiments with varying CCN emissions and concentrations were conducted for the 2015 EPF event. The
3 results illustrate that inclusion of realistic aerosol conditions (less aerosols due to scavenging effect of ongoing rainy
4 conditions) improved the microphysics-dynamics interaction and improved the basin-scale rainfall patterns as
5 simulation biases reduced against IMERG and rain gauge observations. Lower CCN concentrations led to more RWC
6 to CWC ratio at lower atmospheric levels. This shift enhanced warm-rain processes, improving the rainfall magnitude
7 and timing into the basin. Further, rain evaporation processes supported long-term intense cold-pool activity near the
8 basin (Mallinson and Lasher-Trapp, 2019). The persistent cold-pools intensify low-level moisture convergence
9 through thermodynamic forcing, establishing favourable conditions for secondary convection (Schlemmer and
10 Hohenegger, 2014; Schlemmer and Hohenegger, 2016), simulating the bimodal rainfall peaks observed in the basin.
11 In contrast, the simulations with climatological CCN produced an excessive CWC to RWC ratio, causing a premature
12 northward shift of convection and reduced basin accumulated rainfall. Further, LES experiments further demonstrated
13 that under low-CCN conditions, rainfall magnitude and timing improved within the basin, inflow biases were reduced,
14 and inundation extent estimates were enhanced. To summarize, using coupled atmospheric-hydrologic-hydraulic
15 simulations of an EPF event over Chennai on December 1, 2015, the study shows evidence that representation of
16 aerosols at the basin scale can affect the accuracy of EPF prediction and, consequently, urban flooding.

17 From a water resources management perspective, the coupled modeling framework used in this study is required
18 during EPF events. During the 2015 Chennai flood, about one-third of the peak inflow resulted from
19 Chembarambakkam reservoir releases (Nithila Devi et al., 2019; Nithila Devi and Kuiry, 2024). Reducing initial
20 reservoir storage prior to the event could have mitigated the flood impact by 30% and delayed the peak by 12 hours
21 (Panchanthan et al., 2020). Balancing flood mitigation with maintaining adequate reservoir storage during monsoons
22 is crucial. Accurate rainfall prediction, which is the focus of this study, is key to making timely decisions for the
23 reservoirs about water storage or release.

24 While this investigation elucidates the pivotal influence of urban-scale CCN heterogeneity on EPF during the 2015
25 Chennai event, these findings pertain to a single case. This is mainly due to the formidable computational and time
26 requirements of EPF modeling as high-resolution WRF simulations, comprehensive 9-member physics-aerosol
27 ensembles, and computationally exhaustive LES simulations, requiring 100s of core-days per event including regional
28 physics parameterization optima and nested domain configuration. Nevertheless, our rigorous methodological
29 framework establishes quantitative aerosol microphysical plausibility (14-28% rainfall response to coastal CCN
30 gradients) at urban scales. Subsequent investigations should systematically extend this protocol across
31 climatologically diverse EPF archetypes (e.g., Mumbai 2005, Kochi 2018 etc) to rigorously understand aerosol's role
32 on EPF modeling at urban scales which may vary across events and regions.

33

34



1 **Data Availability**

2 The three-hourly aerosol mixing ratio data for the period 2003-2017 were obtained from the Global Modeling and
3 Assimilation Office (GMAO) through the MERRA-2 dataset (inst3_3d_aer_Nv;
4 <https://doi.org/10.5067/LTVB4GPCOTK2>, last access: 30 November 2025). Rainfall data were obtained from the
5 IMERG satellite data (Huffman et al., 2023; <https://doi.org/10.5067/GPM/IMERG/3B-HH/07>, last access: 30
6 November 2025). The accumulated rainfall data used in this study are publicly available on Zenodo
7 <https://doi.org/10.5281/zenodo.17897013> (Paul, 2026).

8 **Supplement**

9 The supplement related to this article is included

10 **Author contributions**

11 C.S. conceived the study along with OP, SNK and KLS. OP and NND performed the simulations. OP analysed the
12 atmospheric results whereas hydrologic-hydraulic results were analysed by NND. OP and NND prepared the first
13 draft. All authors helped in finalizing the manuscript writing.

14 **Competing interests**

15 The authors declare no competing interests for this article.

16 **Acknowledgements**

17 This work has been supported by the Asia-Pacific Network for Global Change Research (APN) (CRRP2022-08MY-
18 Sarangi).

19 **References**

- 20 Barros, A. P., Shrestha, P., Chavez, S., and Duan, Y.: Modeling aerosol-cloud-precipitation interactions in
21 mountainous regions: Challenges in the representation of indirect microphysical effects with impacts at subregional
22 scales, in: Rainfall-extremes, distribution and properties, IntechOpen, <https://doi.org/10.5772/intechopen.80025>,
23 2019.
- 24 Boyaj, A., Ashok, K., Ghosh, S., Devanand, A., and Dandu, G.: The Chennai extreme rainfall event in 2015: The Bay
25 of Bengal connection, *Clim. Dynam.*, 50, 2867-2879, <https://doi.org/10.1007/s00382-017-3778-7>, 2018.
- 26 Brown, J. D., Spencer, T., and Moeller, I.: Modeling storm surge flooding of an urban area with particular reference
27 to modeling uncertainties: A case study of Canvey Island, United Kingdom, *Water Resour. Res.*, 43, W06402,
28 <https://doi.org/10.1029/2005WR004597>, 2007.
- 29 Buchard, V., Randles, C. A., da Silva, A. M., Darmenov, A., Colarco, P. R., Govindaraju, R., Ferrare, R., Hair, J.,
30 Beyersdorf, A. J., Ziemba, L. D., and Yu, H.: The MERRA-2 aerosol reanalysis, 1980 onward. Part II: Evaluation and
31 case studies, *J. Climate*, 30, 6851-6872, <https://doi.org/10.1175/JCLI-D-16-0613.1>, 2017.
- 32 Chakraborty, A.: A synoptic-scale perspective of heavy rainfall over Chennai in November 2015, *Curr. Sci.*, 111, 201-
33 207, <https://doi.org/10.18520/cs/v111/i1/201-207>, 2016.



- 1 Chen, F. and Dudhia, J.: Coupling an advanced land surface–hydrology model with the Penn State–NCAR MM5
2 modeling system. Part I: Model implementation and sensitivity, *Mon. Weather Rev.*, 129, 569–585,
3 [https://doi.org/10.1175/1520-0493\(2001\)129%3C0569:CAALSH%3E2.0.CO;2](https://doi.org/10.1175/1520-0493(2001)129%3C0569:CAALSH%3E2.0.CO;2), 2001.
- 4 Friedl, M. A., McIver, D. K., Hodges, J. C. F., Zhang, X. Y., Muchoney, D., Strahler, A. H., Woodcock, C. E., Gopal,
5 S., Schneider, A., Cooper, A., Baccini, A., Gao, F., and Schaaf, C.: Global land cover mapping from MODIS:
6 Algorithms and early results, *Remote Sens. Environ.*, 83, 287–302, [https://doi.org/10.1016/S0034-4257\(02\)00078-0](https://doi.org/10.1016/S0034-4257(02)00078-0),
7 2002.
- 8 Global Modeling and Assimilation Office (GMAO): MERRA-2 inst3_3d_aer_Nv: 3d, 3-Hourly, Instantaneous,
9 Model-Level, Assimilation, Aerosol Mixing Ratio V5.12.4, NASA GES DISC (last access: 30 November 2025),
10 <https://doi.org/10.5067/LTVB4GPCOTK2>, 2015.
- 11 Ghosh, S., Karmakar, S., Saha, A., Mohanty, P., Ali, S., Satya, K., Raju, V., Krishnakumar, M., Sebastian, R., Behera,
12 R., Ashrit, P. L. N., Murty, K., Srinivas, B., Narasimhan, T., Usha, M. V. R., Murthy, P., Thiruvengadam, J., Indu,
13 D., Thirumalaivasan, J. P., ... Basu, S.: Development of India’s first integrated expert urban flood forecasting system
14 for Chennai, *Curr. Sci.*, 117, 741–745, <https://www.jstor.org/stable/27138336>, 2019.
- 15 Gomez, M., Sharma, S., Reed, S., and Mejia, A.: Skill of ensemble flood inundation forecasts at short- to medium-
16 range timescales, *J. Hydrol.*, 568, 207–220, <https://doi.org/10.1016/j.jhydrol.2018.10.063>, 2019.
- 17 Goswami, B. N., Venugopal, V., Sengupta, D., Madhusoodanan, M. S., and Xavier, P. K.: Increasing trend of extreme
18 rain events over India in a warming environment, *Science*, 314, 1442–1445, <https://doi.org/10.1126/science.1132027>,
19 2006.
- 20 Grell, G. A. and Freitas, S. R.: A scale and aerosol aware stochastic convective parameterization for weather and air
21 quality modeling, *Atmos. Chem. Phys.*, 14, 5233–5250, <https://doi.org/10.5194/acp-14-5233-2014>, 2014.
- 22 Hazra, A., Chaudhari, H. S., Ranalkar, M., and Chen, J. P.: Role of interactions between cloud microphysics, dynamics
23 and aerosol in the heavy rainfall event of June 2013 over Uttarakhand, India, *Q. J. Roy. Meteor. Soc.*, 143, 986–998,
24 <https://doi.org/10.1002/qj.2983>, 2017.
- 25 Huffman, G. J., Stocker, E. F., Bolvin, D. T., Nelkin, E. J., and Tan, J.: GPM IMERG Final precipitation L3 half
26 hourly 0.1° × 0.1° V07, NASA Goddard Earth Sciences Data and Information Services Center (GES DISC), Greenbelt,
27 MD, <https://doi.org/10.5067/GPM/IMERG/3B-HH/07>, (last access: 30 November 2025), 2023.
- 28 Hunter, N. M., Bates, P. D., Neelz, S., Pender, G., Villanueva, I., Wright, N. G., Liang, D., Falconer, R. A., Lin, B.,
29 Waller, S., Crossley, A. J., and Mason, D. C.: Benchmarking 2D hydraulic models for urban flooding, *Proc. Inst. Civ.*
30 *Eng. Water Manag.*, 161, 13–30, <https://doi.org/10.1680/wama.2008.161.1.13>, 2008.
- 31 Konduru, R. T., Mrudula, G., Singh, V., Srivastava, A. K., and Singh, A. K.: Unravelling the causes of 2015 winter
32 monsoon extreme rainfall and floods over Chennai: Influence of atmospheric variability and urbanization on the
33 hydrological cycle, *Urban Clim.*, 47, 101395, <https://doi.org/10.1016/j.uclim.2022.101395>, 2023.
- 34 Kuiry, S. N., Sen, D., and Bates, P. D.: Coupled 1D–Quasi-2D flood inundation model with unstructured grids, *J.*
35 *Hydraul. Eng.*, 136, 493–506, [https://doi.org/10.1061/\(ASCE\)HY.1943-7900.0000211](https://doi.org/10.1061/(ASCE)HY.1943-7900.0000211), 2010.
- 36 Kusaka, H. and Kimura, F.: Coupling a Single-Layer Urban Canopy Model with a Simple Atmospheric Model: Impact
37 on Urban Heat Island Simulation for an Idealized Case, *J. Meteorol. Soc. Jpn.*, 82, 67–80, 2004.



- 1 Kusaka, H., Kondo, H., Kikegawa, Y., and Kimura, F.: A simple single-layer urban canopy model for atmospheric
2 models: Comparison with multi-layer and slab models, *Bound.-Lay. Meteorol.*, 101, 329-358, 2001.
- 3 Laakso, L., Grönholm, T., Rannik, Ü., Kosmale, M., Fiedler, V., Vehkamäki, H., and Kulmala, M.: Ultrafine particle
4 scavenging coefficients calculated from 6 years field measurements, *Atmos. Environ.*, 37, 3605-3613,
5 [https://doi.org/10.1016/S1352-2310\(03\)00326-1](https://doi.org/10.1016/S1352-2310(03)00326-1), 2003.
6
- 7 Lu, C. H., Liu, Q., Wei, S. W., Johnson, B. T., Dang, C., Stegmann, P. G., Grogan, D., Ge, G., Hu, M., and Lueken,
8 M.: The Aerosol Module in the Community Radiative Transfer Model (v2. 2 and v2. 3): accounting for aerosol
9 transmittance effects on the radiance observation operator, *Geosci. Model Dev.*, 15, 1317-1329,
10 <https://doi.org/10.5194/gmd-15-1317-2022>, 2022.
- 11 Lyapustin, A., Wang, Y., Korkin, S., and Huang, D.: MODIS Collection 6 MAIAC algorithm, *Atmos. Meas. Tech.*,
12 11, 5741-5765, <https://doi.org/10.5194/amt-11-5741-2018>, 2018.
- 13 Mallinson, H. M. and Lasher-Trapp, S. G.: An investigation of hydrometeor latent cooling upon convective cold pool
14 formation, sustainment, and properties, *Mon. Weather Rev.*, 147, 3205-3222, <https://doi.org/10.1175/MWR-D-18-0382.1>, 2019.
15
- 16 Mishra, V. and Shah, H. L.: Hydroclimatological perspective of the Kerala flood of 2018, *J. Geol. Soc. India*, 92, 645-
17 650, <https://doi.org/10.1007/s12594-018-1079-3>, 2018.
- 18 Mlawer, E. J., Taubman, S. J., Brown, P. D., Iacono, M. J., and Clough, S. A.: Radiative transfer for inhomogeneous
19 atmospheres: RRTM, a validated correlated-k model for the longwave, *J. Geophys. Res.-Atmos.*, 102, 16663-16682,
20 <https://doi.org/10.1029/97JD00237>, 1997.
- 21 Nakanishi, M., and Niino, H.: Development of an improved turbulence closure model for the atmospheric boundary
22 layer, *J. Meteorol. Soc. Jpn.*, 87, 895-912, <https://doi.org/10.2151/jmsj.87.895>, 2009.
- 23 Narasimhan, B., Bhallamudi, S. M., Mondal, A., Ghosh, S., and Mujumdar, P.: Chennai Floods 2015: A Rapid
24 Assessment, 2016.
- 25 Nithila Devi, N. and Kuiry, S. N.: An urbanization-hydrologic-hydraulic modelling framework for short and long-
26 term flood management strategies, PhD thesis, Indian Institute of Technology Madras, 2023.
- 27 Nithila Devi, N. and Kuiry, S. N.: Evaluation of predictive skill of short-term raw ensemble forecasts for mapping of
28 extreme floods, in: Springer Proc., 163-173, https://doi.org/10.1007/978-981-97-6009-1_17, 2024.
- 29 Nithila Devi, N. and Kuiry, S. N.: Urbanization-informed, uncertainty-based calibration approach for simulating the
30 impact of urbanization on flooding in a data-limited region, *J. Water Clim. Change*, 16, 211-229,
31 <https://doi.org/10.2166/wcc.2025.604>, 2025.
- 32 Nithila Devi, N., Sridharan, B., Bindhu, V. M., Narasimhan, B., Bhallamudi, S. M., Bhatt, C. M., Usha, T., Vasan, D.
33 T., and Kuiry, S. N.: Investigation of Role of Retention Storage in Tanks (Small Water Bodies) on Future Urban
34 Flooding: A Case Study of Chennai City, India, *Water*, 12, 2875, <https://doi.org/10.3390/w12102875>, 2020.
- 35 Nithila Devi, N., Sridharan, B., and Kuiry, S. N.: Impact of urban sprawl on future flooding in Chennai city, India, *J.*
36 *Hydrol.*, 574, 486-496, <https://doi.org/10.1016/j.jhydrol.2019.04.041>, 2019.



- 1 Panchanthan, A., La Rocca, M., and Lakshmanan, E.: Significance of reservoir operation during extreme rainfall event
2 in flood mitigation and water demand management in a metropolitan city of India: a case study, *EGU Gen. Assem.*,
3 <https://doi.org/10.5194/egusphere-egu2020-6409>, 2020.

- 4 Panda, J. and Rath, S. S.: Observed and Simulated Characteristics of 2015 Chennai Heavy Rain Event: Impact of
5 Land-Use Change, SST, and High-Resolution Global Analyses, *Pure Appl. Geophys.*, 179, 3391-3409,
6 <https://doi.org/10.1007/s00024-022-03113-w>, 2022.

- 7 Pattanaik, D. R. and Rajeevan, M.: Variability of extreme rainfall events over India during southwest monsoon season,
8 *Meteorol. Appl.*, 17, 88-104, <https://doi.org/10.1002/met.164>, 2010.

- 9 Paul, O.: Accumulated rainfall data for all sensitivity experiments [Dataset], Zenodo,
10 <https://doi.org/10.5281/zenodo.17897013>, 2026.

- 11 Phadtare, J.: Role of Eastern Ghats orography and cold pool in an extreme rainfall event over Chennai on 1
12 December 2015, *Mon. Weather Rev.*, 146, 943-965, <https://doi.org/10.1175/MWR-D-16-0473.1>, 2018.

- 13 Rai, P. K., Sarangi, C., Arun, N., Kuiry, S. N., and Leung, L. R.: The Dichotomy of Wet and Dry Trends Over India
14 by Aerosol Indirect Effects in CMIP5 Models, *Earth's Future*, 11, <https://doi.org/10.1029/2022EF003266>, 2023.

- 15 Rani, S. I., Arulalan, T., George, J. P., Rajagopal, E. N., Renshaw, R., Maycock, A., Barker, D. M., and Rajeevan, M.:
16 IMDAA: High Resolution Satellite-era Reanalysis for the Indian Monsoon Region, *J. Climate*,
17 <https://doi.org/10.1175/JCLI-D-20-0412.1>, 2021.

- 18 Rath, S. S. and Panda, J.: A Study of Near-Surface Boundary Layer Characteristics During the 2015 Chennai Flood in
19 the Context of Urban-Induced Land Use Changes, *Pure Appl. Geophys.*, 176, 2607-2629,
20 <https://doi.org/10.1007/s00024-018-2069-5>, 2019.

- 21 Reshmi Mohan, P., Srinivas, C. V., Yesubabu, V., Baskaran, R., and Venkatraman, B.: Simulation of a heavy rainfall
22 event over Chennai in Southeast India using WRF: Sensitivity to microphysics parameterization, *Atmos. Res.*, 210,
23 83-99, <https://doi.org/10.1016/j.atmosres.2018.04.005>, 2018.

- 24 Roxy, M. K., Ghosh, S., Pathak, A., Athulya, R., Mujumdar, M., Murtugudde, R., Terray, P., and Rajeevan, M.: A
25 threefold rise in widespread extreme rain events over central India, *Nat. Commun.*, 8, 708,
26 <https://doi.org/10.1038/s41467-017-00744-9>, 2017.

- 27 Sarangi, C., Kanawade, V. P., Tripathi, S. N., Thomas, A., and Ganguly, D.: Aerosol-induced intensification of cooling
28 effect of clouds during Indian summer monsoon, *Nat. Commun.*, 9, 5095, [https://doi.org/10.1038/s41467-018-06015-](https://doi.org/10.1038/s41467-018-06015-5)
29 [5](https://doi.org/10.1038/s41467-018-06015-5), 2018.

- 30 Sarangi, C., Tripathi, S. N., Kanawade, V. P., Koren, I., and Pai, D. S.: Investigation of the aerosol-cloud-rainfall
31 association over the Indian summer monsoon region, *Atmos. Chem. Phys.*, 17, 5185-5204,
32 <https://doi.org/10.5194/acp-17-5185-2017>, 2017.

- 33 Sarangi, C., Tripathi, S. N., Qian, Y., Kumar, S., and Leung, L. R.: Aerosol and Urban Land Use Effect on Rainfall
34 Around Cities in Indo-Gangetic Basin From Observations and Cloud Resolving Model Simulations, *J. Geophys. Res.-*
35 *Atmos.*, 123, 3645-3667, <https://doi.org/10.1002/2017JD028004>, 2018.

- 36 Schlemmer, L. and Hohenegger, C.: The formation of wider and deeper clouds as a result of cold-pool dynamics, *J.*
37 *Atmos. Sci.*, 71, 2842-2858, <https://doi.org/10.1175/JAS-D-13-0170.1>, 2014.



- 1 Schlemmer, L. and Hohenegger, C.: Modifications of the atmospheric moisture field as a result of cold-pool dynamics,
2 Q. J. Roy. Meteor. Soc., 142, 30-42, <https://doi.org/10.1002/qj.2625>, 2016.
- 3 Schubert, J. E. and Sanders, B. F.: Building treatments for urban flood inundation models and implications for
4 predictive skill and modeling efficiency, Adv. Water Resour., 41, 49-64,
5 <https://doi.org/10.1016/j.advwatres.2012.02.012>, 2012.
- 6 Singh, D., Horton, D. E., Tsiang, M., Haugen, M., Ashfaq, M., Mei, R., Diffenbaugh, N. S., and Rajaratnam, B.:
7 Severe precipitation in Northern India in June 2013: Causes, historical context, and changes in probability, Bull. Am.
8 Meteorol. Soc., 95, 1449-1462, 2014.
- 9 Skamarock, W. C., Klemp, J. B., Dudhia, J., Gill, D. O., Barker, D. M., Duda, M. G., Huang, X.-Y., Wang, W., and
10 Powers, J. G.: A Description of the Advanced Research WRF Version 3, NCAR Tech. Note NCAR/TN-475+STR,
11 2008.
- 12 Srinivas, C. V., Yesubabu, V., Hari Prasad, D., Hari Prasad, K. B. R. R., Greeshma, M. M., Baskaran, R., and
13 Venkatraman, B.: Simulation of an extreme heavy rainfall event over Chennai, India using WRF: Sensitivity to grid
14 resolution and boundary layer physics, Atmos. Res., 210, 66-82, <https://doi.org/10.1016/j.atmosres.2018.04.014>,
15 2018.
- 16 Tewari, M., Chen, F., Dudhia, J., Ray, P., Miao, S., Nikolopoulos, E., and Treinish, L.: Understanding the sensitivity
17 of WRF hindcast of Beijing extreme rainfall of 21 July 2012 to microphysics and model initial time, Atmos. Res.,
18 271, 106085, <https://doi.org/10.1016/j.atmosres.2022.106085>, 2022.
- 19 Thompson, G. and Eidhammer, T.: A study of aerosol impacts on clouds and precipitation development in a large
20 winter cyclone, J. Atmos. Sci., 71, 3636-3658, <https://doi.org/10.1175/JAS-D-13-0305.1>, 2014.
- 21 van Oldenborgh, G. J., Otto, F. E. L., Haustein, K., and AchutaRao, K.: The Heavy Precipitation Event of December
22 2015 in Chennai, India, B. Am. Meteorol. Soc., 97, S87-S91, <https://doi.org/10.1175/BAMS-D-16-0129.1>, 2016.
- 23 Virtanen, P., Gommers, R., Oliphant, T. E., Haberland, M., Reddy, T., Cournapeau, D., Burovski, E., Peterson, P.,
24 Weckesser, W., Bright, J., van der Walt, S. J., Brett, M., Wilson, J., Millman, K. J., Mayorov, N., Nelson, A. R. J.,
25 Jones, E., Kern, R., Larson, E., ... Vázquez-Baeza, Y.: SciPy 1.0: Fundamental algorithms for scientific computing in
26 Python, Nat. Methods, 17, 261-272, <https://doi.org/10.1038/s41592-019-0686-2>, 2020.
- 27 Zou, Y. L., Hu, F. L., Zhou, C. C., Li, C. L., and Dunn, K. J.: Analysis of radial basis function interpolation approach,
28 Appl. Geophys., 10, 397-410, <https://doi.org/10.1007/s11770-013-0407-z>, 2013.
- 29
- 30
- 31